Contribution from the Department of Chemistry,
The University of North Carolina, Chapel Hill, North Carolina 27514

Comparisons between Polypyridyl Nitrosyl Complexes of Osmium(II) and Ruthenium(II)

DAVID W. PIPES and THOMAS J. MEYER*

Received August 2, 1983

Comparisons are made between the properties of polypyridyl nitrosyl and nitro complexes of osmium(II) and ruthenium(II) in equivalent coordination environments, e.g., $[(trpy)(bpy)MNO]^{3+}$ and $[(trpy)(bpy)MNO_2]^{+}$ (trpy is 2,2′,2″-terpyridine; bpy is 2,2′-bipyridine). Although there are clear similarities between the two series in terms of properties and reactivities, there are also clear differences. The differences appear to arise from greater Os–NO electronic mixing and greater spin–orbit coupling at Os. Decreased electronic mixing for Ru–NO complexes leads to a more electron-deficient nitrosyl group as shown by enhanced gas-phase affinities both for $e^-(g)$ (~−0.5 V) and for $O^{2-}(g)$ (~−0.71 V) as estimated from solution data. Two ligand-based reductions at the nitrosyl ligand are observed by cyclic voltammetry. For the first reduction, a systematic variation occurs in potential values as the ligand cis to the NO^+ group is varied through the series Cl^-, NO_2^-, py, $^1/_3$ trpy, PPh_3, NH_3, and CH_3CN. $E_{1/2}$ values for the first reduction increase linearly with the energy of the $\nu(NO)$ in a correlation that includes both the Ru and the Os complexes. The chemical and reactivity properties of the Os complexes are similar to those documented earlier for equivalent Ru complexes, including the following: (1) The nitrosyl and nitro complexes are in acid–base equilibrium, $[(trpy)(bpy)Os^{II}NO]^{3+} + 2OH^- \rightleftarrows [(trpy)(bpy)Os^{II}NO_2]^{+} + H_2O$, for which p$K$ = 11 at I = 1.0 M. (2) Oxidation of $[(trpy)(bpy)Os^{II}NO_2]^{+}$ to $[(trpy)(bpy)Os^{III}NO_2]^{2+}$ in acetonitrile at 22.0 ± 0.1 °C is followed by a disproportionation reaction at the nitro ligand, $2[(trpy)(bpy)Os^{III}NO_2]^{2+} \rightarrow [(trpy)(bpy)Os^{II}NO]^{3+} + [(trpy)(bpy)Os^{III}ONO_2]^{2+} + e^-$, which is second order in complex (k_{obsd} = 366 (±58) M^{-1} s^{-1}). (3) In the presence of PPh_3, $[(trpy)(bpy)Os^{III}NO_2]^{2+}$ is captured by PPh_3, $[(trpy)(bpy)Os^{III}NO_2]^{2+} + PPh_3 \rightarrow [(trpy)(bpy)Os^{II}NO]^{2+} + OPPh_3$, before disproportionation can occur.

Introduction

An extensive chemical reactivity toward nucleophiles is known for polypyridyl–nitrosyl complexes of Ru(II), e.g., eq 1–3 (py is pyridine; bpy is 2,2′-bipyridine; Ar is phenyl or a substituted aromatic).[1-3] The spectral and reactivity properties

$$[trans\text{-}(py)_4(Cl)RuNO]^{2+} + N_3^- + H_2O \rightarrow [trans\text{-}(py)_4(Cl)RuOH_2]^{+} + N_2 + N_2O \quad (1)$$

$$[cis\text{-}(bpy)_2(Cl)RuNO]^{2+} + H_2NAr \rightarrow [cis\text{-}(bpy)_2(Cl)RuNNAr]^{2+} + H_2O \quad (2)$$

$$[cis\text{-}(bpy)_2(py)RuNO]^{3+} + (CH_3)_2NC_6H_5 \rightarrow [cis\text{-}(bpy)_2(py)RuN(O)C_6H_4N(CH_3)_2]^{2+} + H^+ \quad (3)$$

of these and other nitrosyl complexes have been reviewed, where it has been noted that a reactivity toward nucleophiles is associated with relatively high $\bar{\nu}(NO)$ stretching energies (>1850 cm^{-1}).[4,5] More recently, the electrochemical reduction of polypyridyl–nitrosyl complexes of both Ru(II) and Os(II) in aqueous solutions has been shown to lead to coordinated NH_3.[1,6]

The goal of the present work was to prepare a series of polypyridyl–nitrosyl complexes of osmium. A major concern was to compare their chemical and physical properties with those for related complexes of ruthenium. Although the two metals are congeners, as a third-row transition metal, osmium has a greater d-orbital extension and spin–orbit coupling becomes a more significant factor in accounting for electronic structure.[7] Nonetheless, the two metals form similar polypyridyl complexes, which provides an interesting opportunity for comparisons between them.

The emphasis here is on the properties of the nitrosyl group, both how such properties vary between the two metals and, for a given metal, how they vary as the ligands are varied. In that sense we regard this as part of a larger study where the goal is to learn the systematics of how ligand variations can be used to transfer chemical reactivity properties from one metal to another.

Experimental Section

Ultraviolet–visible spectra were obtained on a Bausch and Lomb Model 2000 spectrophotometer except for kinetics data, which were obtained on a Varian 634 spectrophotometer. All electrochemical measurements were at platinum electrodes, and all potentials were determined vs. a saturated sodium chloride calomel electrode (SSCE) at 22 ± 1 °C and were uncorrected for junction-potential effects. Potential control for electrochemical experiments was obtained with a Princeton Applied Research Model 175 universal programmer. Cyclic voltammograms were recorded on a Hewlett-Packard Model 7004-B X-Y recorder. Infrared spectra were obtained on a Beckman IR Spectronic 4250, and wavenumber values were measured from polystyrene standards. All pH measurements were done with a Radiometer-Copenhagen PHM62 Standard pH meter with a two-electrode system.

Preparation of Complexes. $(bpy)_2OsCl_2$,[8] $[(bpy)_2(PPh_3)OsNO_2](PF_6)$,[9] $[(bpy)_2(PPh_3)OsNO](PF_6)_3$,[9] and $[(bpy)_3Fe](PF_6)_3$[10] were prepared as described previously. $[(trpy)(bpy)OsCl]^{+}$[11] (trpy is 2,2′,2″-terpyridine) was prepared as described previously except that it was precipitated from aqueous solution as the PF_6^- salt.

$[(trpy)(bpy)OsNO_2](PF_6)$. $[(trpy)(bpy)OsCl](PF_6)$ (0.5 g) was dissolved in a mixture of 3:1 ethylene glycol to water (v/v) (25 mL) under an argon atmosphere. An excess (>20 equiv) of $NaNO_2$ (0.9 g) was added, and the mixture was heated at reflux for 7 h. The solution was cooled to room temperature and one pipetful (2 mL) of saturated aqueous NH_4PF_6 solution (pH >10) added to the solution. The solution was cooled and held at 5 °C for 1 h and filtered. The residue was washed with several milliliters of cold H_2O and then dried under vacuum for 24 h. The compound was purified on an alumina column and eluted with 1:1 acetonitrile–toluene. The eluate was evaporated to a small volume and the product precipitated by the

(1) Bottomley, F.; Mukaida, M. *J. Chem. Soc., Dalton Trans.* **1982**, *10*, 1933–1937.
(2) Meyer, T. J.; Bowden, W. L.; Little, W. F. *J. Am. Chem. Soc.* **1974**, *96*, 5605–5607.
(3) Meyer, T. J.; Bowden, W. L.; Little, W. F. *J. Am. Chem. Soc.* **1976**, *98*, 444–448.
(4) McCleverty, J. A. *Chem. Rev.* **1979**, *79*, 53–76.
(5) Bottomley, F. *Acc. Chem. Res.* **1978**, *11*, 158–162.
(6) Murphy, W. R., Jr.; Takeuchi, K. J.; Meyer, T. J. *J. Am. Chem. Soc.* **1982**, *104*, 5817–5819.
(7) (a) Kober, E. M. Ph.D. Dissertation, The University of North Carolina, Chapel Hill, NC, 1982. (b) Kober, E. M.; Goldsby, K. A.; Narayana, D. N. S.; Meyer, T. J. *J. Am. Chem. Soc.* **1983**, *105*, 4303–4309. (c) Kober, E. M.; Meyer, T. J. *Ibid.* **1982**, *21*, 3967–3977.
(8) Dwyer, F. P.; Buckingham, D. A.; Goodwin, H. A.; Sargeson, A. M. *Aust. J. Chem.* **1964**, *17*, 315–324.
(9) Sullivan, B. P.; Meyer, T. J., unpublished results.
(10) Keene, F. R.; Salmon, D. J.; Walsh, J. L.; Abruña, H. D.; Meyer, T. J. *Inorg. Chem.* **1980**, *19*, 1896–1903.
(11) Buckingham, D. A.; Dwyer, F. P.; Sargeson, A. M. *Aust. J. Chem.* **1964**, *17*, 622–631.

0020-1669/84/1323-2466$01.50/0

Table I. Rate Constant Data for the Disproportionation Reaction $3[(trpy)(bpy)OsNO_2]^{2+} \rightarrow [(trpy)(bpy)OsNO_2]^{+} + [(trpy)(bpy)OsNO]^{3+} + [(trpy)(bpy)OsONO_2]^{2+}$ at 22 ± 0.1 °C in Acetonitrile

run no.	$[Os^{III}NO_2]$- (initial), mM	oxidizing agent	k_{obsd}, M^{-1} s^{-1}
1	0.17	Ce(IV)	313 (±13)[a]
2	0.33	Ce(IV)	358 (±4)
3	0.10	$Fe^{III}(bpy)_3^{3+}$	424 (±17)

[a] The range of observed rate constants for runs at that concentration is in parentheses.

addition of toluene. The solid was collected on a medium frit and dried under vacuum. Anal. Calcd for $[Os(C_{15}H_{11}N_3)(C_{10}H_8N_2)NO_2](PF_6)$: C, 38.96; H, 2.49; N, 10.91. Found: C, 38.98; H, 2.57; N, 10.70.

$[(trpy)(bpy)OsNO](PF_6)_3$. $[(trpy)(bpy)OsNO_2](PF_6)$ (0.3 g) was dissolved in acetonitrile (~10 mL). One milliliter of concentrated HPF_6 (70%) was added slowly with stirring over a 5-min period. The solution was then filtered into an excess of diethyl ether (250 mL). The light yellow precipitate was filtered and air-dried. Further purification was achieved by repeated precipitation from acetonitrile solutions by adding diethyl ether. Anal. Calcd for $[Os(C_{15}H_{11}N_3)(C_{10}H_8N_2)NO](PF_6)_3 \cdot 4H_2O$: C, 26.89; H, 2.44; N, 7.53. Found: C, 26.74; H, 1.96; N, 7.52.

$[(bpy)_2(Cl)OsNO](PF_6)_2$. $(bpy)_2OsCl_2$ (0.2 g) was suspended in 1:1 ethylene glycol–H_2O (5 mL), and the suspension was heated at reflux for 5 h under a nitric oxide atmosphere. The solution was cooled to room temperature, and 1 mL of concentrated HPF_6 was added. After the solution was cooled for 1 h at 5 °C, the product was filtered, washed with diethyl ether, and air-dried. The complex was dissolved in acetonitrile, 1 mL of concentrated HPF_6 was slowly added with stirring, and pure product was precipitated from the solution by addition to an excess volume of diethyl ether. Anal. Calcd for $[Os(C_{10}H_8N_2)_2(Cl)NO](PF_6)_2$: C, 28.00; H, 1.88; N, 8.16. Found: C, 27.90; H, 2.07; N, 7.94.

$(bpy)_2(Cl)OsNO_2$. $[(bpy)_2(Cl)OsNO](PF_6)_2$ (0.1 g) was suspended in aqueous 0.1 M NaOH (5 mL) and the mixture stirred for 1 h. The suspended product was filtered, washed with 1 mL of 0.1 M NaOH, and dried under vacuum. Anal. Calcd for $Os(C_{10}H_8N_2)_2(Cl)NO_2 \cdot H_2O$: C, 39.90; H, 3.02; N, 11.63. Found: C, 39.96; H, 2.93; N, 11.70.

Determination of the Rate Constant for Disproportionation of $[(trpy)(bpy)OsNO_2]^{2+}$. Acetonitrile solutions, 0.1 M in $(NEt_4)(ClO_4)$, containing $[(trpy)(bpy)OsNO_2]^{+}$ and either $(NH_4)_2Ce(NO_3)_6$ or $[(bpy)_3Fe](PF_6)_3$ were mixed in appropriate proportions to give equal molar amounts or a slight excess of $[(trpy)(bpy)OsNO_2]^{+}$. The role of the oxidant was to oxidize Os(II) to Os(III); e.g., $[(bpy)_3Fe]^{3+} + [(trpy)(bpy)OsNO_2]^{+} \rightarrow [(bpy)_3Fe]^{2+} + [(trpy)(bpy)OsNO_2]^{2+}$. After mixing, the solution was added to a 1-cm quartz cuvette and placed in a spectrophotometer. Absorbance changes with time were monitored at λ_{max} (492 nm) for $[(trpy)(bpy)OsNO_2]^{+}$. Appearance of the complex, via eq 4, was rapid, and absorbance changes with time

$$3[(trpy)(bpy)OsNO_2]^{2+} \rightarrow [(trpy)(bpy)OsNO_2]^{+} + [(trpy)(bpy)OsNO]^{3+} + [(trpy)(bpy)OsONO_2]^{2+} \quad (4)$$

were found to follow second-order, equal-concentration kinetics. Rate constants were measured from slopes of plots of $1/(A_\infty - A_t)$ vs. time, where A_t and A_∞ are the absorbances at time t and ∞, respectively. Correlation coefficients were calculated from 95% confidence intervals and were greater than 0.999 for all runs. An average value of k_{obsd} = 366 (±58) M^{-1} s^{-1} was determined from nine kinetic runs at three different concentrations (Table I).

***K* for the Equilibrium $[(trpy)(bpy)OsNO]^{3+} + 2OH^- \rightleftharpoons [(trpy)(bpy)OsNO_2]^{+} + H_2O$.** The equilibrium constant for the nitrosyl–nitro equilibrium was determined spectrophotometrically at 22.0 ± 0.2 °C in H_2O at I = 1.0 M in NaCl. Constant pH was maintained by the use of sodium phosphate buffers (0.05 M). Aliquots of aqueous solutions of $[(trpy)(bpy)OsNO](PF_6)_3$ were added to 10-mL volumetric flasks to give a final concentration of 1.2×10^{-4} M. An aliquot of the buffer solution was added to produce a total buffer concentration of 0.05 M in ionic strength. Final pH adjustments were obtained by addition of 0.1 M NaOH or 0.1 M HCl. Enough NaCl was added to each solution to bring the final ionic strength to 1.0 M. Solutions were allowed to equilibrate for 24 h. Visible spectra (Figure 1) were taken of each solution. Concentrations of $[(trpy)(bpy)OsNO_2]^{+}$ were calculated from absorbance readings at 462 nm, which is the λ_{max} for $[(trpy)(bpy)OsNO_2]^{+}$. The nitrosyl complex is essentially transparent at this wavelength. The concentration of the nitrosyl complex was calculated by mass balance. The pH of each solution was measured by a pH meter standardized by Fischer buffers of pH 7.41 and 10.4. Corrections in pH due to Na^+ ions were adjusted with use of the Radiographic-Copenhagen correction graph supplied with the pH electrodes. Corrections were not greater than +0.04 pH unit. The spectra of seven solutions were obtained between pH 7.40 and 11.01, and the average value of the equilibrium constant found was K(22.0 ± 0.2 °C, I = 1.0 M) = 7.0 (±0.5) × 10^{10} M^{-2}.

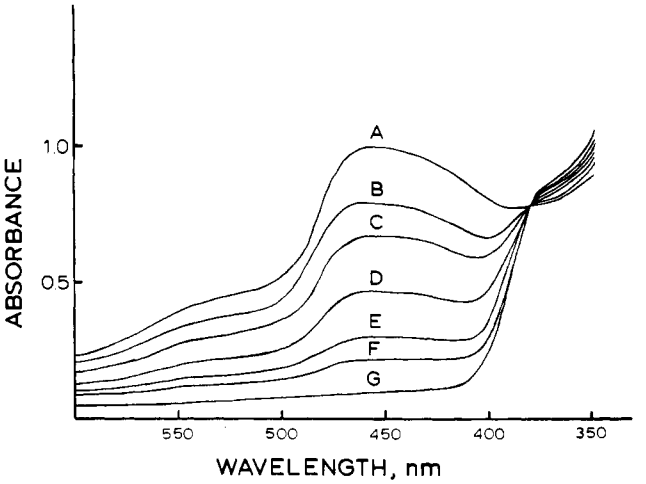

Figure 1. Absorbance spectra for the pH-dependent equilibrium $[(trpy)(bpy)OsNO]^{3+} + 2OH^- \rightleftharpoons [(trpy)(bpy)OsNO_2]^{+} + H_2O$ in aqueous solution (I = 1.0 M NaCl, T = 22.0 ± 0.1 °C) at pH (A) 11.01, (B) 9.08, (C) 8.70, (D) 8.50, (E) 8.37, (F) 8.22, and (G) 7.40.

Table II. Infrared and Electrochemical Data

complex	$\bar{\nu}$(NO),[a] cm^{-1}	$E_{1/2}(1)$[b,c]	$E_{p,c}(2)$[b,d]
$[(trpy)(bpy)OsNO]^{3+}$	1904	−0.02	−0.24[e]
$[(bpy)_2(Cl)OsNO]^{2+}$	1888	−0.30	−0.86
$[(bpy)_2(PPh_3)OsNO]^{3+}$	1898	0.12	−0.57
$[(trpy)(bpy)RuNO]^{3+}$	1952	0.45	−0.20
$[(bpy)_2(Cl)RuNO]^{2+}$ [f]	1940	0.19	−0.60
$[(bpy)_2(py)RuNO]^{3+}$ [f]	1953	0.53	−0.37
$[(bpy)_2(N_3)RuNO]^{2+}$ [f]	1923	0.17	−0.63
$[(bpy)_2(NO_2)RuNO]^{2+}$ [f]	1948	0.33	−0.56
$[(bpy)_2(NH_3)RuNO]^{3+}$ [f]	1950	0.36	−0.48
$[(bpy)_2(CH_3CN)RuNO]^{3+}$ [f]	1970	0.56	−0.35

[a] As wavenumbers in CH_3CN solutions. [b] Potentials measured in volts vs. SSCE (saturated sodium chloride calomel electrode) in 0.1 M TEAP/CH_3CN at a Pt electrode. [c] $E_{1/2}(1)$ is the first nitrosyl-based reduction and is electrochemically reversible. [d] $E_{p,c}(2)$ is the peak potential for the second nitrosyl-based reduction at a scan rate of 200 mV/s. The process is electrochemically irreversible. [e] This is an $E_{1/2}$ value since the couple $[(trpy)(bpy)OsNO]^{2+/+}$ is electrochemically reversible. [f] Values obtained from ref 12.

Attempted Determination of the Rate Constant for the Reaction $[(trpy)(bpy)OsNO_2]^{2+} + PPh_3 \rightarrow [(trpy)(bpy)OsNO]^{2+} + OPPh_3$. Acetonitrile solutions containing $[(trpy)(bpy)OsNO_2]^{+}$ (1.0×10^{-4} M) were oxidized to $[(trpy)(bpy)OsNO_2]^{2+}$ by the addition of 1 equiv of Ce(IV). Immediately following the oxidation, before significant disproportionation could occur, an acetonitrile solution containing excess PPh_3 was added, bringing the final ratio of $[(trpy)(bpy)OsNO_2]^{2+}$ to PPh_3 to 1:5. Absorbance changes vs. time were subsequently recorded as a function of time at 420 nm, which is a λ_{max} for the reduced form of the nitrosyl complex, $[(trpy)(bpy)OsNO]^{2+}$. This reaction was found to be too rapid for the simple mixing technique, and only a lower limit of $k > 350$ M^{-1} s^{-1} could be estimated.

Results

Infrared (ν(NO)) and electrochemical data for NO-based reductions are summarized in Table II.

Table III. Electronic Spectral Data

complex[a]	λ_{max}, nm (ϵ_{max}, M^{-1} cm^{-1})[b] M = Ru	M = Os
$[(trpy)(bpy)MNO_2]^+$	472	492 (10 000)
	310	316
	291	294
$(bpy)_2(Cl)MNO_2$		691[d]
	503 (7500)	506 (8400)
	334 (8700)	430 (9000)
	294 (45 000)	359 (9200)
	237 (20 000)	295 (45 000)
		237 (28 000)
$[(bpy)_2(py)MNO_2]^+$	449 (7800)	
	336 (10 000)	
$[(trpy)(bpy)MNO]^{3+}$	336[c]	370[c]
	305	330 (14 000)
	292 (26 000)	385 (19 000)
$[(bpy)_2(Cl)MNO]^{2+}$	325 (12 500)	325
	294 (17 000)	230

[a] All cations as PF_6^- salts. [b] In CH_3CN. [c] Shoulder. [d] Broad shoulder, see Figure 2.

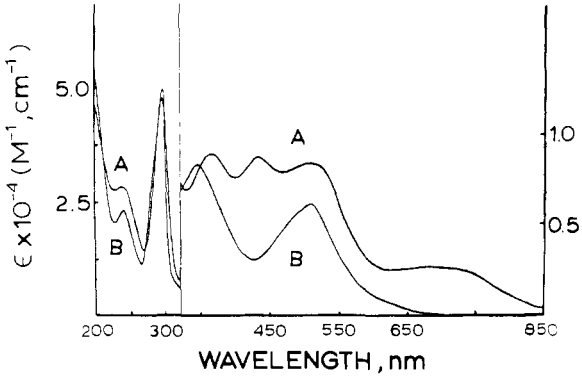

Figure 2. Absorption spectra of (A) $(bpy)_2(Cl)OsNO_2$ and (B) $(bpy)_2(Cl)RuNO_2$ in CH_3CN.

Electronic Spectra. Electronic spectra of polypyridyl complexes of Ru(II) and Os(II) are dominated by intense MLCT, $d\pi(M) \rightarrow \pi^*(bpy)$, absorption bands. The spectra of the Os(II) complexes are generally more complicated than the spectra of the Ru(II) complexes. The large spin–orbit coupling constant for Os(II) leads to significant intensity of singlet → "triplet" transitions because of extensive mixing of the excited singlet and triplet states.[7] Spectroscopic data obtained in acetonitrile solutions are summarized in Table III. The most dramatic effect in comparing osmium nitro and nitrosyl electronic spectra, which is also the case for related Ru complexes, is the absence of visible absorption bands for the nitrosyl complexes. This has been attributed to the effect of strong $d\pi \rightarrow \pi^*(NO)$ back-bonding, which stabilizes the $d\pi$ levels and shifts the MLCT bands into the ultraviolet. It is also important to note that a shoulder appears for the nitrosyl complexes of Os in the range 320–340 nm with an additional shoulder appearing for $[(trpy)(bpy)OsNO]^{3+}$ at 370 nm. For the Ru complexes, related bands also appear in the range 320–340 nm, which have been assigned to $d\pi(Ru(II)) \rightarrow \pi^*(NO)$ transitions on the basis of the results of photochemical experiments. In the photochemical experiments, loss of the NO^+ ligand via the transition $M^{II}–NO^+ \xrightarrow{+h\nu} M^{III}, \dot{N}O$ was achieved by photolysis at these wavelengths.[12]

Acid–Base Equilibria. As for related Ru–nitro/Ru–nitrosyl complex pairs, optical spectra are pH dependent due to an acid–base interconversion between the two forms (eq 5). At

$$[(trpy)(bpy)OsNO]^{3+} + 2OH^- \rightleftharpoons [(trpy)(bpy)OsNO_2]^+ + H_2O \quad (5)$$

intermediate pH values both forms are present and the equilibrium constant can be evaluated as described in the Experimental Section. In Table IV are shown the results of this experiment and of similar measurements on Ru complexes from earlier work.[10,13]

Reactivity of Os(III) Nitro Complexes. Oxidation of polypyridyl–nitro complexes of Ru(II) to Ru(III) is followed by disproportionation apparently by the mechanism shown in Scheme I.[10] However, if an appropriate substrate is available,

Scheme I

$$[(bpy)_2(py)Ru^{II}NO_2]^+ \xrightarrow{-e^-} [(bpy)_2(py)Ru^{III}NO_2]^{2+}$$

$$[(bpy)_2(py)Ru^{III}NO_2]^{2+} \rightleftharpoons [(bpy)_2(py)Ru^{III}ONO]^{2+}$$

$$[(bpy)_2(py)Ru^{III}NO_2]^{2+} + [(bpy)_2(py)Ru^{III}ONO]^{2+} \rightarrow \{[(bpy)_2(py)Ru^{III}N(O)ON(O)ORu^{III}(py)(bpy)_2]^{4+}\} \rightarrow [(bpy)_2(py)Ru^{II}NO]^{3+} + [(bpy)_2(py)Ru^{II}ONO_2]^+$$

$$[(bpy)_2(py)Ru^{III}NO_2]^{2+} + [(bpy)_2(py)Ru^{II}ONO_2]^+ \rightarrow [(bpy)_2(py)Ru^{II}NO_2]^+ + [(bpy)_2(py)Ru^{III}ONO_2]^{2+}$$

such as PPh_3, the $Ru^{III}–NO_2$ intermediate can be captured as shown in eq 6. Both of these reactions have been observed

$$[(bpy)_2(py)Ru^{III}NO_2]^{2+} + PPh_3 \rightarrow [(bpy)_2(py)Ru^{II}\dot{N}O]^{2+} + OPPh_3 \quad (6)$$

for $[(trpy)(bpy)Os^{III}NO_2]^{2+}$. In the first experiment, $[(trpy)(bpy)Os^{II}NO_2]^+$ was oxidized electrochemically at +0.9 V vs. SSCE in the presence of excess PPh_3 in CH_3CN. The product analysis, $OPPh_3$ by infrared ($\nu(P{=}O) = 1180$ cm^{-1}) and $[(trpy)(bpy)Os^{II}\dot{N}O]^{2+}$ by integration of the nitrosyl wave, showed a 1:1 stoichiometry. The sequence of reactions occurring in the presence of PPh_3 is as shown in eq 7–9. At-

$$[(trpy)(bpy)Os^{II}NO_2]^+ \xrightarrow{-e^-} [(trpy)(bpy)Os^{III}NO_2]^{2+} \quad (7)$$

$$[(trpy)(bpy)Os^{III}NO_2]^{2+} + PPh_3 \rightarrow [(trpy)(bpy)Os^{II}\dot{N}O]^{2+} + OPPh_3 \quad (8)$$

$$[(trpy)(bpy)Os^{II}\dot{N}O]^{2+} \xrightarrow{-e^-} [(trpy)(bpy)Os^{II}NO]^{3+} \quad (9)$$

tempts to measure a rate constant for the redox step in eq 8 were unsuccessful. However, a lower limit of $k_{obsd} > 350$ M^{-1} s^{-1} (22.0 ± 0.1 °C) can be estimated for the reaction, which can be compared to $k_{obsd} = 200$ M^{-1} s^{-1} for the oxidation of PPh_3 by $[(bpy)_2(Cl)Ru^{III}NO_2]^{2+}$ under the same conditions as measured by chronoamperometry in 0.1 M TBAH.[14]

Following oxidation of $[(trpy)(bpy)Os^{II}NO_2]^+$ to Os(III), the ligand-based disproportionation reaction in eq 4 occurs. The stoichiometry in eq 4 was shown by coulometry ($n = 1.5$)[10] and by the appearance of the products in approximately equal amounts by integrated peak areas: $E_{1/2}([(trpy)(bpy)OsNO_2]^{2+/+}) = 0.71$ V, $E_{1/2}([(trpy)(bpy)OsONO_2]^{2+/+}) = 0.60$ V, $E_{1/2}([(trpy)(bpy)OsNO]^{3+/2+}) = -0.02$ V. The rate constant for the redox step was determined by kinetic experiments with either $(NH_4)_2Ce^{IV}(NO_3)_6$ or $[Fe(bpy)_3](PF_6)_3$ as the oxidant. After mixing, absorbance changes with time were observed at 492 nm, which is a λ_{max} for $[(trpy)(bpy)OsNO_2]^+$. The absorbance changes and the second-order,

(12) Callahan, R. W.; Meyer, T. J. *Inorg. Chem.* **1977**, *16*, 574–581.

(13) Thompson, M. S. Ph.D. Dissertation, The University of North Carolina, Chapel Hill, NC, 1982.

(14) Keene, F. R.; Salmon, D. J.; Meyer, T. J. *J. Am. Chem. Soc.* **1977**, *99*, 4821–4822.

Scheme II

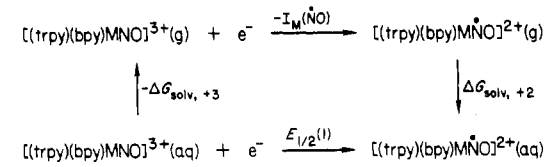

equal-concentration kinetics observed for the absorbance changes with time were consistent with the reactions

$$[(trpy)(bpy)Os^{II}NO_2]^+ + Ce(IV) \xrightarrow{fast} [(trpy)(bpy)Os^{III}NO_2]^{2+} + Ce(III)$$

$$2[(trpy)(bpy)Os^{III}NO_2]^{2+} \rightarrow [(trpy)(bpy)Os^{II}NO]^{3+} + [(trpy)(bpy)Os^{II}ONO_2]^+$$

$$[(trpy)(bpy)Os^{III}NO_2]^{2+} + [(trpy)(bpy)Os^{II}ONO_2]^+ \xrightarrow{fast} [(trpy)(bpy)Os^{II}NO_2]^+ + [(trpy)(bpy)Os^{III}ONO_2]^+$$

Rate constants for the rate-determining step were obtained from plots of $1/\Delta A$ vs. time, where $\Delta A = A_\infty - A_t$ (A_t and A_∞ are the absorbances at times t and ∞, respectively). From nine runs, $k(22 \pm 0.2\ ^\circ C, I = 0.1\ M) = 366\ (\pm 58)\ M^{-1}\ s^{-1}$.

Discussion

The original theme of this paper was to compare the properties and reactivities of closely related ruthenium and osmium nitrosyl complexes. At the same time the results provide an excellent opportunity to address in a subtle way the differences between the two metals in equivalent coordination environments and to view their influence on the nitrosyl ligand.

In Table II are summarized $E_{1/2}(1)$ and $E_{p,c}(2)$ values for the reduction of a series of nitrosyl complexes. As noted in earlier work, the first, chemically reversible reduction occurs at an orbital largely π^*(NO) in character, as indicated by a shift to lower energy of 300 cm^{-1} in the ν(NO) stretching vibration.[12] From the data obtained here and earlier, systematic variations in $E_{1/2}(1)$ occur as the ligand cis to the nitrosyl group is varied. From the data in Table II it is also clear that significant variations occur with a change in the metal for equivalent coordination environments. In fact, when viewed in the context of the thermodynamic cycle in Scheme II, such comparisons can be very revealing. Given the similar ionic radii for Os(II/III) compared to Ru(II/III),[15] the molecular volumes of the Ru and Os complexes that appear in Scheme II are nearly the same and so the solvation energy terms, $-\Delta G_{solv,+3}$ and $\Delta G_{solv,+2}$ in the scheme are expected to be nearly the same for Ru and Os complexes having equivalent coordination environments.

As a consequence, as shown in eq 10, the difference in $E_{1/2}(1)$ values between equivalent Ru and Os complexes, 0.47 V for the $[(trpy)(bpy)MNO]^{3+/2+}$ couples and 0.49 V for the $[(bpy)_2(Cl)MNO]^{2+/+}$ couples, is an approximate measure of the difference in the electron affinities of the nitrosyl groups in the gas phase as measured by their ionization energies ($I_M(\dot{N}O)$). The difference of ca. 0.5 V shows that, in

$$E_{1/2}(1)_{Ru} - E_{1/2}(1)_{Os} \simeq I_{Ru}(\dot{N}O) - I_{Os}(\dot{N}O) \simeq 0.5\ V \quad (10)$$

equivalent nitrosyl complexes of Ru and Os, the π^*(NO) level in the Os complex is 0.5 V higher in energy (nearer the free electron in a vacuum) than is the Ru complex.

From $E_{1/2}$ measurements on equivalent $(bpy)_2M^{III/II}L_2$ couples for Ru and Os, $E_{1/2}$ values for the Ru couples are generally more positive by 0.4–0.5 V.[16] Once again, given the similarities expected in molecular volumes and common charge types, a cycle like that in Scheme II shows that, for the metal-based couples, difference in gas-phase ionization energies for the M(II) ions can be estimated from $E_{1/2}(Ru(III/II)) - E_{1/2}(Os(III/II)) = \Delta E_{1/2} \simeq I(Ru^{II}) - I(Os^{II})$, where $I(Ru^{II})$ and $I(Os^{II})$ are the gas-phase ionization energies. From the $E_{1/2}$ values, the suggestion can be made that $I(Ru^{III}) - I(Os^{III}) \simeq 0.4$–0.5 V. As noted by Sargeson and Buckingham, a contributing factor in such comparisons is the fact that the third ionization energies (I_3) for the free gas-phase ions is significantly lower for Os (25.0 V) than for Ru (28.4 V).[16]

Chart I. $E^{\circ\prime}$ Values in V in CH_3CN at 22 (±1) °C vs. SSCE

$E^{\circ\prime}$	redox couples	electronic nature of the couple
−0.30	$[(bpy)_2(Cl)OsNO]^{2+/+}$	Os-N⁺O/Os-ṄO
0.0	SSCE	
0.19	$[(bpy)_2(Cl)RuNO]^{2+/+}$	Ru-N⁺O/Ru-ṄO
0.28	$[(bpy)_2(Cl)OsNH_2R]^{2+/+}$ [a]	Os^{III}/Os^{II}
0.70	$[(bpy)_2(Cl)RuNH_2R]^{2+/+}$ [b]	Ru^{III}/Ru^{II}
1.4	$NO^{+/0}$ [c]	
3.0	$[(bpy)_2(Cl)RuNO]^{3+/2+}$ [d]	Ru^{III}/Ru^{II}

[a] R is adamantyl, $-C_{10}H_{15}$.[21] [b] R is *tert*-butyl, $-C(CH_3)_3$.[22] [c] $E^{\circ\prime}$ measured in nitromethane. [d] $E^{\circ\prime}$ measured in liquid SO_2.[19]

With the available redox potential data at hand it is possible to assess in a semiquantitative fashion the consequences of metal nitrosyl bond formation for the two metals in equivalent coordination environments. The points to be made are based on the data in the redox potential diagram in Chart I. In the redox potential diagram, the potentials are arranged in increasing order so as to approach the value for the free electron in vacuum at −4.8 V vs. SSCE as the reference. Included in the scheme are potentials for $M^{III/II}$ couples of the type $[(bpy)_2(Cl)M(NH_2R)]^{2+/+}$. They are included as cases where the ligand cis to the chloro group is a non-π-back-bonding primary amine. The value for the NO^+/NO couple is taken from the literature,[18] and the value for the couple $[(bpy)_2(Cl)Ru^{III}(NO)]^{3+}/[(bpy)_2(Cl)Ru^{II}(NO)]^{2+}$ was measured in liquid SO_2.[19] Although a value for the analogous $Os^{III/II}$ couple is not known, the observation of $d\pi \rightarrow \pi^*$(NO) optical transitions in the region 320–380 nm (Table III) for both the Ru and the Os complexes suggests that the potential for the $Os^{III/II}$ couple may be in the same range.

It is not possible to make detailed comparisons based on the data in Chart I because of variations in charge types and the conditions used for the measurements. Nevertheless, it is clear that the effect of metal–nitrosyl bonding on the dπ(M) levels compared to that of, for example, a primary amine as ligand is profound. The importance of $d\pi-\pi^*$ back-bonding in complexes of Ru(II) has been discussed in detail by Taube.[20] In this context it is obvious that the nitrosyl ligand plays a special role as evidenced by the increase in Ru(III/II) potential of 2.3 V in comparing the $[(bpy)_2(Cl)RuNH_2R]^{2+/+}$ and $[(bpy)_2(Cl)RuNO]^{3+/2+}$ couples.

(15) Griffith, W. P. "The Chemistry of the Rare Platinum Metals", Interscience: New York, 1967; Chapters 2–4.
(16) Buckingham, D. A.; Sargeson, A. M. "Chelating Agents and Metal Chelates"; Dwyer, F. P., Miller, D. P., Eds.; Academic Press: New York, 1964; pp 237–280.
(17) Bard, A. J.; Faulkner, L. R. "Electrochemical Methods"; Wiley: New York, 1980; pp 633–634.
(18) Bauer, D.; Foucault, A. *J. Electroanal. Chem. Interfacial Electrochem.* **1972**, *39*, 377–384. Cauquis, G.; Serve, D. *C. R. Seances Acad. Sci.* **1968**, *266*, 1591–1594.
(19) Abruña, H., private communication.
(20) Taube, H. *Surv. Prog. Chem.* **1973**, *6*, 1–46.
(21) Gilbert, J. A.; Meyer, T. J., unpublished results.
(22) Takeuchi, K. J.; Meyer, T. J., unpublished results.

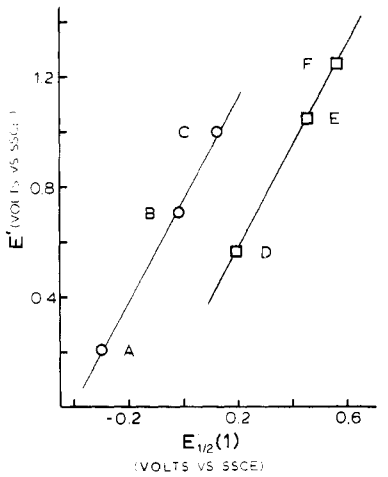

Figure 3. Plots of reduction potentials, E' (a mixture of $E_{1/2}$ and $E_{p,a}$ values), for the $M^{III/II}NO_2$ couples for polypyridyl nitro complexes of Ru and Os vs. the first ligand-based reduction potential, $E_{1/2}(1)$, for the analogous nitrosyl complexes. The complexes listed are in order of increasing E' and $E_{1/2}(1)$. For the Os complexes (○) the sets of couples are (A) $[(bpy)_2(Cl)OsNO_2]^{+/0}/[(bpy)_2(Cl)OsNO]^{2+/+}$, (B) $[(trpy)(bpy)OsNO_2]^{2+/+}/[(trpy)(bpy)OsNO]^{3+/2+}$, and (C) $[(bpy)_2(PPh_3)OsNO_2]^{2+/+}/[(bpy)_2(PPh_3)OsNO]^{3+/2+}$. For Ru (□) the couples are (D) $[(bpy)_2(Cl)RuNO_2]^{+/0}/[(bpy)_2(Cl)RuNO]^{2+/+}$, (E) $[(trpy)(bpy)RuNO_2]^{2+/+}/[(trpy)(bpy)RuNO]^{3+/2+}$, and (F) $[(bpy)_2(PPh_3)RuNO_2]^{2+/+}/[(bpy)_2(PPh_3)RuNO]^{3+/2+}$.

It is equally interesting to note the effects on the nitrosyl ligand of the change in metals between Ru and Os. The NO^+ ion is a relatively powerful oxidant. In the Os and Ru complexes, the largely NO-based reductions occur at lower potentials compared to those of NO^+ because of net M → NO electron donation to form the M–NO bond. As noted above, the effect of M–NO bonding at the metal is profound as shown by the shift in Ru(III/II) potential positively by ~2.3 V compared to the shift for the relatively innocent primary amine ligand. Clearly, metal→NO^+ bonding leads to significant changes at the ligand as well, but in a chemical sense the ligand still retains a considerable NO^+ character. This is shown by the redox potential data in Chart I and by the characteristic NO^+-like reactivity of the ruthenium nitrosyl complexes, e.g., eq 1–3.

Returning to the data in Chart I, it is interesting to note that the difference in potentials for the metal-based $[(bpy)_2(Cl)M(NH_2R)]^{2+/+}$ couples (0.42 V) is approximately maintained in the potential differences between the ligand-based $[(bpy)_2(Cl)MNO]^{2+/+}$ couples (0.49 V). What this suggests is that the relatively large shift to more negative potentials for NO^+ bound to Os(II) may be largely a consequence of the fact that the dπ levels are nearer π*(NO) rather than a consequence of the larger 5d compared to 4d radial extension for Os(II). In any case, the net effect is an enhanced Os–NO mixing compared to that for Ru–NO in equivalent coordination environments.

Comparisons between Ru and Os in terms of the effects of ligand variations are possible, for both the metal-based $M^{III}NO_2/M^{II}NO_2$ couples and the ligand-based $M^{II}NO^+/M^{II}NO$ couples. In making such comparisons, one should note that potentials for the $M^{III/II}NO_2$ couples are a mixture of $E_{1/2}$ and $E_{p,a}$ values. In some cases only $E_{p,a}$ is available because of the rapid chemical step involving NO_2^--based ligand disproportionation (eq 4). For the sake of argument, we will take the $E_{p,a}$ values as reasonable estimates for $E_{1/2}$ values.

In order to make comparisons based on ligand variations, it is of value to plot redox potentials for the $M^{II}NO_2$ oxidation vs. potentials for $M(NO^+)$-based reductions as shown in Figure 3. One advantage of such a plot is that it compensates in part for the differences that arise from different charge types between the various couples. As can be seen from the plot in Figure 3, potentials for the $M^{III/II}NO_2$ and $M^{II}(NO^{+/0})$ couples vary linearly as the ligand cis to the nitrosyl and nitro group is varied. For the two types of couples, variations in the ligand L in *cis*-$(bpy)_2(L)MNO_2$ are expected to influence the potential for the metal-based $M^{III/II}NO_2$ couples by a combination of σ-bonding and π-back-bonding effects. Oxidation state II (d^6) is expected to be stabilized, in a relative sense, by dπ → π*(L) back-bonding in the presence of added ligands having low-lying dπ* levels like PPh_3 or vacant π* levels like pyridine, $^1/_3$ terpyridine, and NO_2^-. Oxidation state III (d^5) is expected to be stabilized by σ-donor and/or π-donor ligands like Cl^-. The linear correlations between the $M^{III/II}NO_2$ and $M^{II}NO^{+/0}$ potentials suggest that the redox level which is largely π*(NO) in character varies in the same way as the cis ligands are varied. However, the slopes of the correlations are significantly greater than 1 (1.8), showing that the effects of variations in L on the π*(NO) levels are less than on the dπ levels, which is not surprising given the largely ligand-based character of the redox level. The effects of variations in L on the π*(NO)-based reductions must arise largely from electronic stabilization effects in the $[(bpy)_2(L)M(NO^+)]^{n+}$ form of the couple and are probably a direct reflection of the importance of dπ–π*(NO) back-bonding but as felt indirectly by variations in an adjacent ligand.

Clearly from the data in Table II, significant variations also occur for the second, nitrosyl-based reductions, for example, $[(bpy)_2(py)Ru(NO)]^{2+} + e^- \rightarrow [(bpy)_2(py)Ru(NO^-)]^+$. However, with the exception of the $[Os(trpy)(bpy)NO]^{2+/+}$ couple, at the scan rate used (200 mV/s) the other couples are chemically and electrochemically irreversible. The chemistry that occurs following the second, irreversible reduction is related to that observed earlier in the net reduction of bound NO^+ to NH_3 and is currently under investigation.[1,6]

A second point of note concerning the correlation in Figure 3 is that the variations in $E_{1/2}(M^{III/II}NO_2)$ potentials with $E_{1/2}(1)$ give parallel lines, one for Ru and one for Os. A conclusion which can be drawn is that, following formation of the M–NO bond, secondary variations in the M–NO electronic structure induced by ligand variations at the cis position are the same in magnitude for either metal.

Given the same similarities in properties and in variations with L for related Ru and Os complexes, it is of interest to consider those variations in the remaining ligands which, at least in principle, would lead to a "chemical interconversion" between the two metals as evidenced, for example, by similar $E_{1/2}$ values. This issue can be addressed on the basis of the data in Figure 3. Consider, for example, the variations in ligands at Os which would lead to a π*(NO)-based potential for $E_{1/2}(1)$ of approximately the same value as for a corresponding Ru complex. Experimentally, this point is reached at Os for the complex $[(bpy)_2(PPh_3)OsNO]^{3+}$ when compared to $[(bpy)_2(Cl)RuNO]^{2+}$. There is an equivalency in $E_{1/2}(1)$ values between M = Os, L = PPh_3 and M = Ru, L = Cl^-, and as a consequence, the chemical properties at the bound NO ligand may be closely related in the two complexes. However, as can be seen by comparing $M^{III/II}$ potentials for the related nitro complexes, the synthetic changes that interconvert Ru and Os in terms of reduction at the NO^+ ligand lead at the same time to a significant change in $E_{1/2}$ values for the $M^{III/II}NO_2$ couples. The point is that although systematic variations in L can lead to a coincidence in $E_{1/2}(1)$ values (or even $E_{p,c}(2)$ value), because of the nearly parallel relationship between the lines in Figure 3, *no variation in L can lead to a complex where both* $E_{1/2}(III/II)$ *and* $E_{1/2}(1)$ *are the same.* A complete chemical interconversion between the two metals in terms of their redox characteristics cannot be made by variations in their ligands.

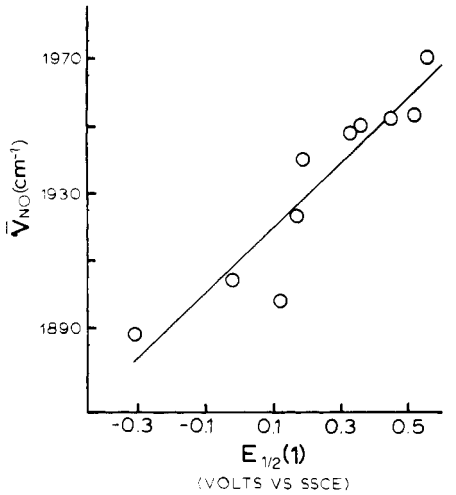

Figure 4. Plot of nitrosyl stretching frequency, $\bar{\nu}$(NO) (cm^{-1}), vs. the first nitrosyl-based reduction potential, $E_{1/2}(1)$ (V vs. SSCE), for polypyridyl–nitrosyl complexes of Os(II) and Ru(II) in CH_3CN. The individual values are tabulated in Table II.

Scheme III

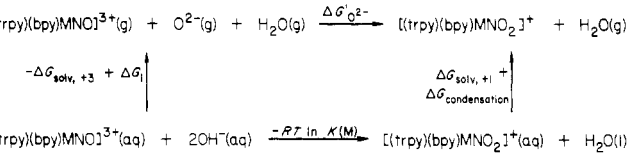

Correlations between $\bar{\nu}$(NO) and $E_{1/2}(1)$ Induced by Ligand Variations. The point was made in the previous section that the effects of ligand variations on dπ levels at Ru(II) is paralleled by variations in π^*(NO) levels as evidenced by the data in Figure 4. In the bonding sense, such correlations point to the importance of dπ–π^*(NO) back-bonding. They suggest that variations in π^*(NO) as evidenced by the $E_{1/2}(1)$ data in Table II should be paralleled by changes in $\bar{\nu}$(NO) as variations are made in the ligand cis to the NO group, since both should respond to changes in dπ–π^* back-bonding. In Figure 4 is shown a plot of $\bar{\nu}$(NO) vs. $E_{1/2}(1)$ for the extended series of M–NO complexes (Table II). Although there is a significant scattering of the experimental points from the least-squares line (y intercept 1909 cm^{-1}, slope 97 cm^{-1}/V) shown in the figure, experimentally, a linear trend clearly exists between $\bar{\nu}$(NO) and $E_{1/2}(1)$. There is no obvious reason for the significant deviation of $[(bpy)_2(PPh_3)OsNO]^{3+}$ from the line, although it may be related to the effect on $E_{1/2}(1)$ of the introduction of the large hydrophobic ligand, PPh_3, near the nitrosyl group. It is also worth noting, once again, that the relatively low values of $E_{1/2}(1)$ and $\bar{\nu}$(NO) for the Os complexes are clear indications of the greater extent of dπ-(Os)–π^*(NO) mixing for Os compared to Ru. A linear correlation between $\bar{\nu}$(NO) and the potential for a ligand-based reduction have been reported for the series of complexes *trans*-$(dppe)_2(L)MoNO$, L = PhCN, MeCN, CNO^-, SCN^-, I^-, H^-, N_3^-, and OH^- (dppe = $Ph_2PCH_2CH_2PPh_2$) by Chatt.[23]

pK Values for the M(NO)/M(NO_2) Acid–Base Equilibrium. As noted in the Results, pK values have been obtained for the acid–base M(NO)/M(NO_2) equilibria for several Ru and Os complexes, e.g., eq 11. As is evident from the somewhat

$$[(trpy)(bpy)RuNO]^{3+} + 2OH^- \rightleftharpoons [(trpy)(bpy)RuNO_2]^+ + H_2O \quad (11)$$

limited data in Table IV, the magnitude of pK is dependent both upon the metal and on the cis ligand. The factors involved in determining the magnitude of the K values can be discussed using the thermodynamic cycle in Scheme III. The most straightforward comparison to make is for Ru compared to Os in a common coordination environment where the solvation energy terms, $\Delta G_{solv,+3}$ and $\Delta G_{solv,+1}$, are expected to be nearly the same. Given this fact, it is possible to estimate relative gas-phase affinities of the coordinated nitrosyl groups at Os compared to those at Ru on the basis of the K values in Table IV, $\Delta G_{O^{2-}}(Ru) - \Delta G_{O^{2-}}(Os) = -RT \ln [K(Ru)/K(Os)] = -0.71$ V. The comparison is of value since it allows relative gas-phase affinities for the bound nitrosyl group toward e(g) (−0.46 V) and O^{2-}(g) (−0.71 V) to be made. Once again, the higher affinity of both entities for a nitrosyl group bound to a Ru compared to that for NO bound to Os is no doubt a direct reflection of a greater electron deficiency because of decreased dπ(Ru)–π^*(NO) mixing.

It is interesting to note that pK values for $[(bpy)_2(Cl)RuNO]^{2+}$ and $[(trpy)(bpy)OsNO]^{3+}$ are comparable in magnitude. The nearly equivalent acidities for Os compared to Ru in the different coordination environments arises from two effects. One is that the Ru complex is more electron rich as a consequence of substitution of Cl^- for a pyridyl-type ligand, and second, there are important differences in solvation energies because of the different charge types involved between the two acid-based pairs.

$M^{III}NO_2$ (M = Ru, Os) Complexes as Two-Electron Oxidants. Given the pK values and the data for the potentials of the $M^{III}NO_2/M^{II}NO_2$ and $M^{II}N^+O/M^{II}NO$ couples, it is possible to calculate formal potentials for the $M^{III}NO_2$ complexes as two-electron, oxygen donor (O atom) oxidants (eq 12).[10] The data used in the calculations were obtained in

$$[(trpy)(bpy)Os^{III}NO_2]^{2+} + H_2O + 2e^- \rightarrow [(trpy)(bpy)Os^{II}NO]^{2+} + 2OH^- \quad (12)$$

aqueous 1 M NaCl, and values for several Ru couples and for the $[(trpy)(bpy)Os^{III}NO_2]^{2+}$ couple are shown in Table V.

In order to make kinetic comparisons between $Ru^{III}NO_2$ and

Table IV. Acid–Base Equilibrium Constants at 22.0 + 0.1 °C in 1.0 M NaCl

reacn	K, M^{-2}	pK	pH[c]
$[(bpy)_2(Cl)RuNO]^{2+} + 2OH^- \rightleftharpoons (bpy)_2(Cl)RuNO_2 + H_2O$	1.6×10^9 [a]	9.2	9.4
$[(bpy)_2(py)RuNO]^{3+} + 2OH^- \rightleftharpoons [(bpy)_2(py)RuNO_2]^+ + H_2O$	1.0×10^{20} [a]	20	4.0
$[(trpy)(bpy)RuNO]^{3+} + 2OH^- \rightleftharpoons [(trpy)(bpy)RuNO_2]^+ + H_2O$	2.1×10^{23} [b]	23	2.3
$[(trpy)(bpy)OsNO]^{3+} + 2OH^- \rightleftharpoons [(trpy)(bpy)OsNO_2]^+ + H_2O$	7.0×10^{10}	11	8.6

[a] From ref 10. [b] From ref 24. [c] Approximate pH at which the nitro and nitrosyl forms are present in equal amounts.

Table V. Rate Constant and Formal Potentials for O Atom Transfer Reactions

redox couple	$E^{\circ\prime}$, V[a]	k_{PPh_3}, M^{-1} s^{-1} [b]	k_{dis}[c]
$[(bpy)_2(Cl)Ru^{III}NO_2]^+/[(bpy)_2(Cl)Ru^{II}NO]^+$	0.31	200 (±11)	(4.2 ± 0.1) × 10^{-3} s^{-1}
$[(trpy)(bpy)Ru^{III}NO_2]^{2+}/[(trpy)(bpy)Ru^{II}NO]^{2+}$	0.14		
$[(bpy)_2(py)Ru^{III}NO_2]^{2+}/[(bpy)_2(py)Ru^{II}NO]^{2+}$	0.26		
$[(trpy)(bpy)Os^{III}NO_2]^{2+}/[(trpy)(bpy)Os^{II}NO]^{2+}$	0.10	>350	366 (±58) M^{-1} s^{-1}

[a] Values measured vs. NHE at I = 1.0 M (NaCl) at 22.0 ± 0.1 °C and pH 14. [b] Second-order rate constant for the oxidation of PPh_3 by $M^{III}NO_2$, $M^{III}NO_2 + PPh_3 \rightarrow M^{II}NO + OPPh_3$, in CH_3CN at 22.0 ± 0.1 °C. [c] First- or second-order rate constant for ligand-based disproportionation, $2M^{III}NO_2 \rightarrow M^{II}N^+O + M^{III}ONO_2 + e^-$, in CH_3CN at 22.0 ± 0.1 °C.

(23) Chatt, J. *Coord. Chem. Rev.* **1982**, *43*, 337–347.
(24) Abruña, H. D.; Walsh, J. L.; Meyer, T. J.; Murray, R. W. *J. Am. Chem. Soc.* **1980**, *102*, 3272–3274.

$Os^{III}NO_2$ complexes as $2e^-$ oxidants, we have investigated both the oxidation of PPh_3 and the disproportionation reaction based on $[(trpy)(bpy)Os^{III}NO_2]^{2+}$.

(1) Oxidation of PPh_3. The details of the experiment were described earlier, where it was noted that the oxidation is quantitative as shown in eq 13. Rate constant comparisons

$$[(trpy)(bpy)Os^{III}NO_2]^{2+} + PPh_3 \rightarrow [(trpy)(bpy)Os^{II}\dot{N}O]^{2+} + OPPh_3 \quad (13)$$

in Table V show that unfortunately only a lower limit could be obtained for the rate constant for the oxidation of PPh_3 by $Os^{III}NO_2^{2+}$ with $k > 350\ M^{-1}\ s^{-1}$.

(2) Disproportionation of Bound NO_2^-. Following oxidation of $[(trpy)(bpy)Os^{II}NO_2]^+$ to $[(trpy)(bpy)Os^{III}NO_2]^{2+}$, disproportionation of the bound nitro group occurs according to eq 4 as described in Results. The kinetics of the ligand-based disproportionation reaction were studied by oxidation of $[(trpy)(bpy)Os^{II}NO_2]^+$ with use of $(NH_4)_2Ce^{IV}(NO_3)_6$ or $(bpy)_3Fe^{III}(PF_6)_3$ and monitoring of the subsequent spectral changes. For the $Ru^{III}NO_2$ complexes, a detailed mechanism has evolved based on the combination of electrochemical and spectral measurement shown in Scheme I. The importance of such couples has been demonstrated in earlier work, where two-electron pathways involving net oxygen atom transfer have been invoked, for example, in the catalytic oxidation of PPh_3 and in the ligand-based disproportionation reaction involving the coordinated NO_2^- ligand shown in eq 14.[10,14] One of the

$$3[(bpy)_2(Cl)Ru^{III}NO_2]^+ \rightarrow (bpy)_2(Cl)Ru^{II}NO_2 + [(bpy)_2(Cl)Ru^{III}ONO_2]^+ + [(bpy)_2(Cl)Ru^{II}NO]^{2+} \quad (14)$$

interesting features about the O atom pathway is that it appears to take advantage of the O-donating ability of the nitro group and the electron-acceptor ability of both metal (Ru(III)) and ligand ($Ru(NO^+)$) sites, $[(bpy)_2(Cl)Ru^{III}NO_2]^+ + PPh_3 \rightarrow [(bpy)_2(Cl)Ru{-}N(O)\cdots O(2e^-)\cdots PPh_3^+] \rightarrow [(bpy)_2(Cl)Ru^{II}NO]^+ + O{=}PPh_3$. For the complexes, $[(bpy)_2(py)RuNO_2]^{2+}$ and $[(trpy)(bpy)RuNO_2]^{2+}$, the reactions are too rapid to obtain kinetic data. For $[(bpy)_2(Cl)RuNO_2]^+$, the kinetics are first order, suggesting that the isomerization step, $Ru^{III}NO_2 \rightleftharpoons Ru^{III}ONO$, is the rate-determining step. Stoichiometric studies with $[(trpy)(bpy)Os^{III}NO_2]^{2+}$, as shown in eq 4, suggest that the net chemistry for both Ru and Os is the same. However, the kinetics study on the disproportionation of $OsNO_2$ shows that, in contrast to $[(bpy)_2(Cl)Ru^{III}NO_2]^+$, the rate law is second order in Os(III). Assuming that the net mechanism for NO_2^- disproportionation remains the same for the $Os^{III}NO_2$ complex, the detailed mechanism of the ligand redox steps would becomes as shown in Scheme IV. Note that from cyclic voltammetry there is no evidence for the presence of $Os^{III}ONO$ on the time scale of the electrochemical experiment, and so if the intermediate is present, it must be present in small amounts. To be consistent with both the rate and the cyclic voltammetric data the mechanism must involve a rapid preequilibrium followed by oxidation of $Os^{III}ONO$ by $Os^{III}NO_2$, in which case, $k_{dis} = kK$, where k is the rate constant for the redox step. The failure of $Os^{III}ONO^{2+}$ to appear by cyclic voltammetry suggests that $K < 0.1$. Note that direct evidence for the appearance of ruthenium nitrito ($Ru^{III}ONO$) complexes has been obtained in low-temperature cyclic voltammetric experiments.[24]

Scheme IV

$$[(trpy)(bpy)Os^{III}NO_2]^{2+} \overset{K}{\rightleftharpoons} [(trpy)(bpy)Os^{III}ONO]^{2+}$$

$$[(trpy)(bpy)Os^{III}NO_2]^{2+} + [(trpy)(bpy)Os^{III}ONO]^{2+} \xrightarrow{k} [(trpy)(bpy)Os^{II}NO]^{3+} + [(trpy)(bpy)Os^{II}ONO_2]^+ \quad (15)$$

One of the themes of this paper has been to compare properties ($E^{\circ\prime}$, pK_a, k_{dis}, $\bar{\nu}(NO)$, etc.) between Ru and Os in equivalent coordination environments. The two reactions above allow the comparison to be extended to O-atom type reactions, and the following points should be noted: (1) In the oxidation of PPh_3, $k([(trpy)(bpy)Os^{III}NO_2]^{2+}) > k([(bpy)_2(Cl)Ru^{III}NO_2]^+)$ even though the potential for the two-electron couple is considerably in favor of the Ru complex as an oxidant: at pH 7, $E^{\circ\prime}(Os^{III}NO_2/Os^{II}\dot{N}O) = 0.52$ V and $E^{\circ\prime}(Ru^{III}(Cl)NO_2/Ru^{II}(Cl)\dot{N}O) = 0.72$ V. This observation would appear to disfavor an initial one-electron step in the oxidation of PPh_3 (eq 16). For the oxidation, net O-atom

$$[(trpy)(bpy)Os^{III}NO_2]^{2+} + PPh_3 \rightarrow [(trpy)(bpy)Os^{II}NO_2]^+ + PPh_3^{-}\cdot \quad (16)$$

transfer is known to occur for $Ru^{III}NO_2$ as shown from ^{18}O-labeling studies.[14] Assuming that the Ru and Os mechanisms both involve O-atom transfers, the comparison in rate constants is striking and important since it suggests that equivalent Os complexes are kinetically considerably more facile in the type of reaction pathway shown in eq 17. The apparent redox

$$M^{III}NO_2 + PPh_3 \rightarrow [M^{III}{-}N(O)\cdots O\cdots PPh_3] \rightarrow M^{II}\dot{N}O + OPPh_3 \quad (17)$$

labilization of the N–O bond toward transfer of an O atom may be another manifestation of enhanced M–NO mixing for the Os(II) products. However, detailed conclusions are limited by other factors, including the fact that the kinetics measurements were made in CH_3CN and the $E^{\circ\prime}$ values in H_2O. (2) For the ligand-based disproportionation reaction, if it is assumed that the overall mechanisms for M = Ru and Os are the same, then the striking feature is the change in rate-determining step. For $[(bpy)_2(Cl)Ru^{III}NO_2]^+$, the rate-determining step is the isomerization step, $Ru^{III}NO_2 \rightleftharpoons Ru^{III}ONO$, with $k_{obsd} = 2 \times 10^{-3}\ s^{-1}$, while for $[(trpy)(bpy)Os^{III}NO_2]^{2+}$ the rate-determining step is the second-order redox reaction. In order to be consistent with the rate law and concentration conditions, the interconversion $Os^{III}NO_2 \rightleftharpoons Os^{III}ONO$ must be facile and it can be estimated from our kinetics data that, in CH_3CN at 22.0 ± 0.1 °C, $k > 0.2\ s^{-1}$ for the interconversion. Here again, there is an interesting change in reactivity properties in comparing Ru and Os.

Acknowledgment is made to the National Science Foundation under Grant No. CHE-8002433 and the National Institutes of Health under Grant No. 1-R01-GM32296-01 for support of this research.

Registry No. $[(trpy)(bpy)OsNO_2](PF_6)$, 90219-14-0; $[(trpy)(bpy)OsNO](PF_6)_3$, 90219-15-1; $[(bpy)_2(Cl)OsNO](PF_6)_2$, 81846-96-0; $(bpy)_2(Cl)OsNO_2$, 90219-16-2; $[(bpy)_2(PPh_3)OsNO]^{3+}$, 90219-17-3; $[(trpy)(bpy)RuNO]^{3+}$, 78913-53-8; $[(trpy)(bpy)OsCl](PF_6)$, 89576-34-1; $(bpy)_2OsCl_2$, 15702-72-4; $[(trpy)(bpy)RuNO_2]^+$, 78913-50-5; $(bpy)_2(Cl)RuNO_2$, 34398-51-1; $[(bpy)_2(py)RuNO_2]^+$, 34398-55-5; $[(bpy)_2(Cl)RuNO]^{2+}$, 52690-88-7; $[(trpy)(bpy)OsNO_2]^{2+}$, 90219-18-4; PPh_3, 603-35-0; $[(trpy)(bpy)OsNO]^{2+}$, 90219-19-5; $[(bpy)_2(Cl)OsNO]^+$, 90219-20-8; $[(bpy)_2(Cl)RuNO]^+$, 54866-04-5; $[(bpy)_2(py)RuNO]^{3+}$, 82769-10-6; $[(bpy)_2(Cl)Ru^{III}NO_2]^+$, 63771-54-0; $[(trpy)(bpy)Ru^{III}NO_2]^{2+}$, 90219-21-9; $[(trpy)(bpy)Ru^{II}NO]^{2+}$, 90219-22-0; $[(bpy)_2(py)Ru^{III}NO_2]^{2+}$, 63771-55-1; $[(bpy)_2(py)Ru^{II}NO]^{2+}$, 72378-59-7; NO_2^-, 14797-65-0.